The Zebrafish *fade out* Mutant: A Novel Genetic Model for Hermansky–Pudlak Syndrome

Ronja Bahadori,[1] *Oliver Rinner,*[1,2] *Helia Berrit Schonthaler,*[1,3] *Oliver Biehlmaier,*[1,3] *Yuri V. Makhankov,*[1,3] *Prashanth Rao,*[4] *Pudur Jagadeeswaran,*[4] *and Stephan C. F. Neuhauss*[1,3]

Purpose. To characterize retinal morphology and visual system function in the zebrafish mutant *fade out* (*fad*) and to establish the mutant as a lower vertebrate model for Hermansky–Pudlak syndrome (HPS).

Methods. Retinal morphology of *fad* larvae was examined between 3 and 9 days postfertilization (dpf) by standard histology, transmission electron microscopy, and immunohistochemistry examination. Apoptotic cells were visualized by TdT-mediated dUTP nick-end labeling (TUNEL) staining. Visual system function was probed by electroretinography and behavioral assessment by optokinetic response measurements. Blood clotting was evaluated by time to occlusion testing of blood vessels as an arterial thrombosis assay. The chromosomal location of *fad* was determined by simple sequence-length polymorphism mapping. Genomic fragments of candidate genes were cloned by standard molecular techniques and mapped to the zebrafish genome by radiation hybrid mapping.

Results. Mutant *fad* larvae are hypopigmented and show structural defects in the outer retina. Melanosomes of these larvae in the retinal pigment epithelium are hypopigmented, generally smaller, and progressively reduced in number compared to nonmutant larvae. Progressive microvilli protrusions into the photoreceptor cell layer are not detectable, and photoreceptor outer segments get shorter and are misaligned. Photoreceptors subsequently undergo apoptosis, with a peak of cell death at 6 dpf. Electrical responses of the retina and visual performance are severely reduced. Blood clotting is prolonged in mutant *fad* larvae. Genomic mapping of *fad* reveals distinct genomic positions of the mutant gene from known human HPS genes.

Conclusions. The *fad* mutant shows syndromic defects in pigmentation, outer retinal structure and function, and blood clotting. This syndrome is characteristic of Hermansky–Pudlak syndrome (HPS), making *fad* a novel genetic model of HPS. The gene does not cosegregate with the known human HPS genes, suggesting a novel molecular cause of HPS. (*Invest Ophthalmol Vis Sci.* 2006;47:4523–4531) DOI:10.1167/iovs.05-1596

Hermansky–Pudlak syndrome (HPS) is a group of autosomal recessive disorders characterized by oculocutaneous albinism and platelet storage pool deficiency.[1–3] Oculocutaneous albinism in these disorders is characterized by various degrees of hypopigmentation of the skin, retinal pigment epithelium (RPE) of the eye, congenital nystagmus, and reduced visual acuity.[4–6] Additionally, the lack of dense granules in platelets is associated with impaired platelet function as indicated by decreased aggregation response, which causes platelet storage pool deficiency.[7,8] HPS is manifested by defects in synthesis, processing, or trafficking of lysosome-related organelles (LROs), most notably melanosomes and platelet-dense granules.[2,3,9–11] These organelles share a variety of features with lysosomes, such as acidic interiors, high intragranular Ca^{2+} concentrations, and resident lysosomal hydrolases.[12]

Human platelets contain three to eight dense granules per platelet[13,14] that play a central role in homeostasis and thrombosis. Dense granules have a highly condensed core that contains serotonin, Ca^{2+}, adenosine triphosphate (ATP), adenosine diphosphate (ADP), and pyrophosphate. Serotonin of dense granules causes vasocontraction and is involved in the formation of the hemostatic plug.[15]

Intracellular melanosomes are the sites of synthesis and storage of melanin pigment in pigment cells of the body (melanocytes in mammals, melanophores in fish and amphibians) and the RPE, where they line the back of the eye.

RPE cells are essential for the function and survival of photoreceptors. They function in the transport of nutrients and circadian phagocytosis of the shed photoreceptor outer segments.[16] Furthermore, the outer segments are stabilized by microvilli, and the outgrowth of the photoreceptor outer segments is guided by the finger-like structure of the microvilli.[17] In zebrafish the absence of microvilli leads to misaligned, collapsed, and shorter photoreceptor outer segments.[18] Additionally, evidence indicates trophic support of photoreceptors, and RPE cells directly support vision by taking part in the recycling of visual pigment.[19,20]

To date, 7 genes in humans and 14 genes in mice that cause HPS have been identified (for reviews, see Huizing et al.[10] and Li et al.[21]). Although the functions of many of these genes remain unknown, several have been shown to be involved in various aspects of trafficking proteins to nascent organelles, particularly lysosomal and late lysosomal organelles.

In a large-scale chemical mutagenesis screen in zebrafish, an extensive collection of mutants with defects in body and eye pigmentation were identified.[22,23] A subsequent behavioral screen for defects in vision identified a number of hypopigmented mutants with deficits in visual performance.[24] One of these mutants was the recessive mutant *fade out* (*fad*). In *fad*, early melanophores initially appear to form normally, but, beginning at 4 days postfertilization (dpf), they appear to be hypopigmented. These hypopigmented larvae exhibit little or no response to visual stimuli at 5 dpf.[24]

From the [1]Swiss Federal Institute of Technology (ETH), Department of Biology, and Brain Research Institute, and the [3]Institute of Zoology, University of Zurich, Zurich, Switzerland; and the [4]Department of Biological Sciences, University of North Texas, Denton, Texas.

[2]Present affiliation: Swiss Federal Institute of Technology, Institute of Systemsbiology, University of Zurich, Zurich, Switzerland.

Supported by the Swiss National Science Foundation (SNF), the Velux Foundation (SCFN, OB), the Roche Research Foundation (OR), the EMBO Young Investigator Program (SCFN), and ETH internal grants (RB, HBS, YVM).

Submitted for publication December 15, 2005; revised May 30, 2006; accepted July 27, 2006.

Disclosure: **R. Bahadori**, None; **O. Rinner**, None; **H.B. Schonthaler**, None; **O. Biehlmaier**, None; **Y.V. Makhankov**, None; **P. Rao**, None; **P. Jagadeeswaran**, None; **S.C.F. Neuhauss**, None

The publication costs of this article were defrayed in part by page charge payment. This article must therefore be marked "*advertisement*" in accordance with 18 U.S.C. §1734 solely to indicate this fact.

Corresponding author: Stephan C. F. Neuhauss, Institute of Zoology, University of Zurich, Winterthurerstrasse 190, CH-8057 Zurich, Switzerland; stephan.neuhauss@zool.unizh.ch.

In this study, we characterized the visual system defect of homozygote *fad* larvae by using behavioral, electrophysiologic, and histologic criteria. We found a progressive decrease in visual system performance paralleled by morphologic defects of the outer retina. Melanosomes in the RPE became progressively abnormal in shape and pigmentation, and microvilli were absent, likely causing misaligned and shorter photoreceptor outer segments. Photoreceptors subsequently died by apoptosis, ultimately leading to complete blindness of the larvae.

The defect in *fad* is not limited to pigmentation and the visual system because homozygous larvae exhibit a prolonged occlusion time of blood vessels in an arterial thrombosis assay, thereby showing all the characteristics of Hermansky–Pudlak syndrome.

We located the mutant locus to zebrafish linkage group 2, whereas all seven orthologs of human *HPS* genes mapped to different linkage groups. Our data established the zebrafish mutant *fad* as a lower vertebrate model for Hermansky–Pudlak syndrome, possibly caused by a novel gene defect.

METHODS

All experiments were conducted in compliance with the ARVO Statement for the Use of Animals in Ophthalmic and Vision Research.

Fish Maintenance and Breeding

Fish were raised and crossed as previously described.[25] Outcrossed sibling pairs were set up to identify heterozygous carriers. Clutches of these identification crosses were used for phenotypic analysis. Embryos were raised at 28°C in E3 medium (5 mM NaCl, 0.17 mM KCl, 0.33 mM $CaCl^2$, and 0.33 mM $MgSO^4$) and were staged according to development in days post fertilization (dpf).[26] All data in this study were obtained using the *fade out*^{tm63c} allele.

Optokinetic Response Measurements

Psychophysical measurements of visual performance were taken as described.[27] Briefly, to measure eye velocity, single larvae were placed dorsal side up in the center of a Petri dish (35-mm diameter) containing 3% prewarmed (28°C) methylcellulose. Moving sine-wave gratings were projected (4200 DLP; ASK Proxima, Wilsonville, OR) onto a screen within the visual field of the larva, at an apparent distance 4.65 cm from the larva's right eye. Projection size on the screen was 8×6 cm, subtending a visual angle of 65.6° horizontally and 53.1° vertically. Eye movements triggered by the visual stimulation were recorded by means of an infrared-sensitive CCD camera. Custom-developed software (LabView IMAQ, version 5.1; National Instruments, Austin, TX) was used to control stimulation and camera and to analyze the resultant images.

Contrast sensitivity functions for wild-type and mutant larvae were measured by the gain (eye velocity/grating velocity) as function of the spatial frequency of the moving grating with alternate movement direction (0.33 Hz). Averaged eye velocity for each spatial frequency was calculated by integration of eye velocity traces.

Electroretinographic Recordings

Electroretinograms (ERGs) were performed on larvae at 5 dpf, as previously described.[28] Briefly, all specimens were dark adapted for 30 minutes before they were positioned in the recording chamber. Each larva was placed on its side on the surface of a moist sponge with E3 medium (5 mM NaCl, 0.17 mM KCl, 0.33 mM $CaCl_2$ and 0.33 mM $MgSO_4$) and was paralyzed by a droplet of muscle relaxant (0.8 mg/mL in larval medium; Esmeron; Organon Teknika, Eppelheim, Germany). The Ag/AgCl electrode system was used to record the ERG response. The recording electrode was positioned in the center of the cornea. The reference Ag/AgCl pellet was placed under the body of the larva. A 5-minute period was chosen to adapt the larva to dark before measurement. The duration of light stimulus was 100 msec, and the interstimulus interval was 5 seconds. Light stimulus was fixed at five relatively different light intensities of 2 lux (OD 4) to 20 klux (OD 0). A virtual instrument (VI) was developed (LabView 5.1; National Instruments) for use in all experiments. Sampling was performed in buffered acquisition mode at a sampling rate of 250 Hz.

Histology

Paraformaldehyde-fixed larvae (4% paraformaldehyde in 0.2 M phosphate buffer, pH 7.4, for 1 hour at room temperature) were dehydrated in a graded series of ethanol-water mixtures, then incubated in 1:1 and 1:3 ethanol and basic solution (Technovit 7100; Heraeus Kulzer, Hanau, Germany) for 1 hour each. After overnight infiltration in basic solution, larvae were positioned in polymerization medium (Technovit 7100; Heraeus Kulzer) overnight at room temperature.

Microtome sections (3 μm) were prepared and mounted on slides (SuperFrost Plus; Menzel-Gläser, Braunschweig, Germany), air dried at 60°C, stained with toluidine blue solution (0.1% in distilled water), overlaid with rapid mounting medium (Entellan; Merck, Darmstadt, Germany), and coverslipped. Some larvae used for histology were raised in 0.2 mM phenylthiourea (Sigma, St. Louis, MO) to inhibit pigment formation.

Electron Microscopy

Embryos were fixed in 2% (wt/vol) paraformalddehyde/2% glutaraldehyde in 0.2 M phosphate buffer (PB; pH 7.2) overnight and were postfixed in 1% osmium tetroxide for 1 hour. After a rinse in 0.1 M PB, specimens were dehydrated in a graded series of ethanol-water mixtures up to 70% ethanol and then contrasted in 2% uranyl and 70% ethanol acetate overnight. On the following day, ethanol dehydration was continued to 100%. After preinfiltration in 1:1 100% ethanol/embedding resin (Fluka, Buchs, Switzerland), larvae were infiltrated in pure embedding resin overnight. Larvae were then positioned in Beem caps with fresh resin and polymerized at 60°C for approximately 16 hours. Ultrathin transverse sections 60-nm thick were prepared and stained with lead citrate. Sections were examined and photographed with a transmission electron microscope (model EM; Carl Zeiss, Oberkochen, Germany).

Immunohistochemistry

Fixed larvae were cryoprotected in 30% sucrose for at least 2 hours. Whole larvae were embedded in tissue-freezing medium (Cryomatrix; Jung-Leica; Thermo Electron Corp., Waltham, MA) and rapidly frozen in liquid N_2; 25-μm thick sections were cut at −20°C, mounted on slides (SuperFrost Plus; Menzel-Gläser), and air dried at 37°C for at least 2 hours. The slides were stored at −20°C until further use. For immunohistochemistry, slides were thawed, washed three times in phosphate-buffered saline (PBS; 50 mM), pH 7.4, and treated with 20% normal goat serum (NGS) and 2% bovine serum albumin (BSA) in PBS/0.3% Triton X-100 (PBST) for 1 hour. Sections were then incubated overnight in primary antibody in PBST at 4°C. Mouse anti–glutamine synthetase (1:700; Chemicon International, Temecula, CA), zpr1 (1:100; University of Oregon Stockcenter), zn8 (1:500; University of Oregon Stockcenter), and 25 kDa rabbit antisynaptosomal-associated protein (1:300, SNAP-25; StressGen, San Diego, CA) were used as primary antibody. After three washes in PBST, sections were incubated in anti–mouse Alexa433– coupled antibody (1:500; Jackson Laboratory, Bar Harbor, ME) for 1 hour, washed three times in PBST, mounted in glycerol, and analyzed under a fluorescence microscope (Axioscope; Carl Zeiss).

Cell Death Detection

The TUNEL (terminal deoxynucleotidyl transferase [TdT]-mediated deoxyuridinetriphosphate [dUTP] nick end-labeling) method[29] was used to identify cells undergoing apoptosis, as previously described.[30] Cryosections were cut 40-μm thick and mounted on slides (SuperFrost Plus; Menzel-Gläser). Quantification was performed by counting apoptotic

cells in one section per eye with the maximal number of apoptotic cells. Significance levels were calculated using a two-tailed paired *t* test.

Arterial Thrombosis Assay

Homozygote *fad* mutant larvae were selected 5 to 6 dpf by their lighter appearance and by observations of the RPE to identify functional defects of thrombocytes with the arterial thrombosis assay. As controls, larvae with normal pigmentation from the same clutch were used. Arterial thrombosis was induced as described previously by injuring a region of dorsal aorta at the fifth somite, located caudal to the anal pore.[31] Time to occlusion (TTO) of the vessel was measured by counting from the time of injury to complete vascular occlusion. The prolongation of TTO compared with controls indicated a defect in thrombocyte function.

Genomic Mapping

The *fade out* (*fad*) mutant was identified in a genetic background of the Tübingen strain further outcrossed to the WIK strain for the mapping procedure. DNA of the F2 homozygous mutants and siblings were analyzed by PCR in pooled-segregate analysis, as described earlier.[32] The mutation was assigned to linkage group 2 with a panel of 192 simple sequence-length polymorphism (SSLP) markers distributed over the entire genome. The linkage group assignation and the precise map position were confirmed by segregation analysis on single embryos. The more precise map position was obtained with the use of additional polymorphic single-length polymorphisms.

Identification of Candidate Genes and Radiation Hybrid Mapping

Candidate orthologs of human Hermansky–Pudlak syndrome genes were identified by tblastn[33] against EST libraries and the annotated zebrafish genomic sequence (http://www.ensembl.org). Orthology of predicted ortholog transcripts was confirmed by comparison of exon/intron structure between the human genes and the predicted transcripts. Transcript numbers on the zv5 release (http://www.sanger.ac.uk/Projects/D_rerio) were: HPS1, ENSDARP00000057047; HPS2, ENSDARG00000013040; HPS3, ENSDARG00000015749; HPS4, ENSDARG00000015749; HPS5 (5′), GENSCAN00000016286; HPS5 (3′), ENSDARG00000027920; HPS6, ENSDARG00000013581; HPS7, ENSDARG00000005024.

Zebrafish orthologs of all seven HPS genes were mapped on the Goodfellow T51 radiation hybrid (RH) panel.[34] The following primers were designed for the seven *Hps* zebrafish ortholog genes: *Hps1*-fw (tgtatgtggattgtcacaggg), *Hps1*-rev (ttctagatctaccccatgaaaccc); *Hps2*-fw (ctacaggaatgaagtctgaagg), *Hps2*-rev (ttctttccattggcaatgagc); *Hps3*-fw (gcggcagactctgagcgagcag), *Hps3*-rev (tggtggcgtgcagcaatacctg); *Hps4*-fw (gatgctaacctggcttatgatt), *Hps4*-rev (gacaatggcctcctgtagtgt); *Hps5*-fw (tctggcgtgtgggtaataagg), *Hps5*-rev (ccagcagctgtttgaactgg); *Hps6*-fw (cttccctgagcctcgaattgg), *Hps6*-rev (atactcgtcacggtcatgtcc); *Hps6*-fw (aggcctaacgcgataatgcaa), *Hps6*-rev (cgtgtgacacaagtcgcagag); *Hps7*-fw (gcaaacacgacgtatagctgt), *Hps7*-rev (gaactgcagcctgcgacttta).

PCR was run on the RH panel, and for all markers it was independently performed in duplicate.

Results

The zebrafish mutant *fad* is characterized by reduced pigmentation of the body melanophores and the RPE. It was initially identified in a large-scale mutagenesis screen and was classified as a melanophore degradation mutant.[22] Pigmentation of the melanophores and RPE is initially normal but becomes hypopigmented and fragmented during subsequent development. At 6 dpf, the homozygote *fad* mutant larvae (Fig. 1A) can readily be distinguished from their wild-type siblings because of their lighter appearance (Fig. 1C). In the mutant, the melanosomes located in the RPE and the melanophores become pale and patchy. Figures 1B and 1D depict the shapes of melanophores in the head region at higher magnification in the wild-type and *fad* larvae. These changes became more severe with ongoing development, leading to nearly unpigmented larvae at 9 dpf. Mutant larvae died approximately 10 dpf.

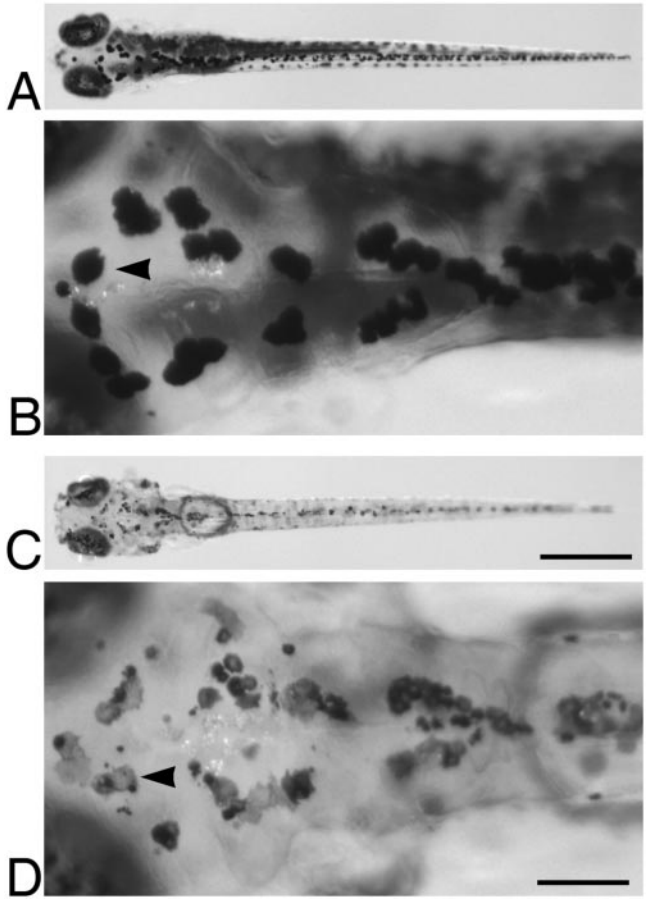

Figure 1. External phenotype of *fad*. Hypopigmented homozygous *fad* mutant (**A**) and heterozygous wild-type sibling (**C**) at 6 dpf. At higher magnification, the *fad* mutant (**B**) compared with the wild-type (**D**) revealed changes in the shape and melanosome distribution of body melanophores. (**B**, **D**, *arrowheads*) Melanophores of the dorsal head region. Scale bars: (**C**) 500 μm; (**D**) 200 μm.

Visual Performance of *fade out*

The defect in visual abilities in the *fad* larvae was previously investigated.[24] To quantify the visual loss, we measured the eye velocity at different spatial frequencies.

Plotting the optokinetic gain as a function of the stimulus spatial frequency yields the contrast sensitivity function (CSF), a commonly used psychophysical function to examine the state of the visual system. The CSF is influenced not only by the geometry and the optical quality of the eye but also by receptor spacing and spatial and temporal visual integration. It is, therefore, a comprehensive measure of visual performance. CSF was measured in larvae at 5 dpf and 8 dpf ($n = 9$). Spatial frequency of the grating stimulus varied between 0.025 and 0.16 c/deg. All measurements were performed under a moderate mean luminance of 42 cd/m^2, a pattern contrast of 85%, and a grating velocity of 7.5 deg/s.

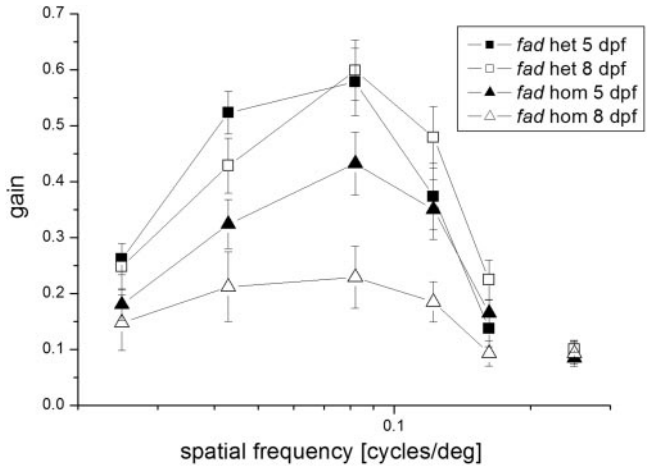

FIGURE 2. Behavioral contrast-sensitivity function of mutant (*triangles*, $n = 9$) and wild-type (*squares*, $n = 9$) *fad* larvae at 5 dpf and 8 dpf. Optokinetic gain was measured as a function of grating spatial frequency. Offset indicates the base levels of the gain. At 5 dpf, the gain was slightly reduced in homozygous larvae compared with their heterozygous siblings. At 8 dpf, mutant *fad* showed a markedly reduced optokinetic response and a lower high-frequency cutoff. Error bars indicate SEM.

Consistent with the progressive pigmentation loss, visual performance was strongly reduced at later developmental stages. At 5 dpf, the visual performance of *fad* mutants was only slightly reduced compared with their wild-type siblings (Fig. 2). At 8 dpf, optokinetic gain and visual acuity were severely reduced in *fad* mutants. Optokinetic gain was reduced 62%. At the maximum measured spatial frequency visible for wild-type larvae (0.16 c/deg), visual response was no longer detectable in *fad* homozygous larvae. Because the behavioral data indicated a loss of visual performance, we set out to test outer retinal function directly by recording ERGs at 5 dpf. We recorded 5 dpf *fad* homozygous and heterozygous larvae because at this stage the ERG can be reliably measured in zebrafish larvae.[28,35,36] The *fad* ($n = 5$) larvae were compared with their siblings ($n = 6$). ERG responses of *fad* larvae (Fig. 3A) were weaker, and no clear a-wave was recordable, in contrast to typical ERG recordings in siblings (Fig. 3B). We compared b-wave amplitudes between mutant and sibling larvae at the two highest light intensities, where the mutants displayed visible b-waves, and the differences were striking (200 ± 46.1 vs. 30 ± 32 at OD1 and 167 ± 38.2 vs. 20 ± 13.2 at OD2) and highly significant (Fig. 3).

Histologic Analysis of the *fad* Retina

Hypopigmentation in combination with our data on behavioral and electrophysiologic impairment suggested a morphologic defect of the *fad* retina. With the use of standard histology, we analyzed the retinas of homozygous and unaffected wild-type siblings between 3 and 9 dpf.

At 3 dpf, formation of the photoreceptor cell (PRC) outer segments was initiated.[37] At the same stage, the retina of the homozygous *fad* larvae could not be differentiated from that of their heterozygous siblings (Fig. 4A, 4B).

At 5 dpf, all major cell types could be identified in the retina, and the separation of the retinal layers was completed. The RPE was filled with melanin-containing melanosomes, and outer segments of photoreceptors were clearly visible in the wild-type larvae (Fig. 4C). In the *fad* larvae, the retina was equally well layered, but the RPE was hypopigmented and melanin clots were apparent (Fig. 4D).

As development proceeded, the RPE phenotype became progressively more severe. The density of melanosomes in the RPE of mutant larvae (Fig. 4F) was decreased in comparison with their wild-type siblings (Fig. 4E). At 9 dpf, the RPE of the *fad* retina contained only a few melanin granules in the periphery, whereas the central part of the RPE was completely devoid of pigmented cells (Fig. 4H).

The outer segments of the PRCs also became severely affected, presumably as a consequence of the changes in the RPE. At 5 dpf, the PRC outer segments appeared shorter than in wild-type (Fig. 4D, arrowhead). At 7 dpf, the outer segments were absent in some parts of the retina (Fig. 4F). The defect was more severe in central regions than in the periphery, suggesting an age-dependent progression.

To identify whether PRCs were affected, we labeled these cells with zpr1, an antibody that labels red/green double cones, the most prevalent photoreceptor subtype in early larval retina.[38] At 5 dpf, the distribution of double cones was uniform throughout the retina (Fig. 5D). However, at 9 dpf, photoreceptor immunoreactivity was patchy and decreased, consistent with PRC death (Fig. 5H).

To label inner retinal cells on further investigation, we used various antibodies such as glutamine synthethase (a Müller glia-specific marker), presynaptic SNAP-25 protein (synaptosomal-associated protein 25 kDa), and zn8 (recognizing the neurolin protein in the ganglion cell layer). In the mutant retina at 7 and 9 dpf, Müller glia cell morphology with elongated cell bodies and processes spanning the entire inner retina[39] was preserved in the mutant. We could not observe any defects when we used antibodies for staining of the ganglion cell epitope zn8 and presynaptic SNAP-25 protein (data not shown).

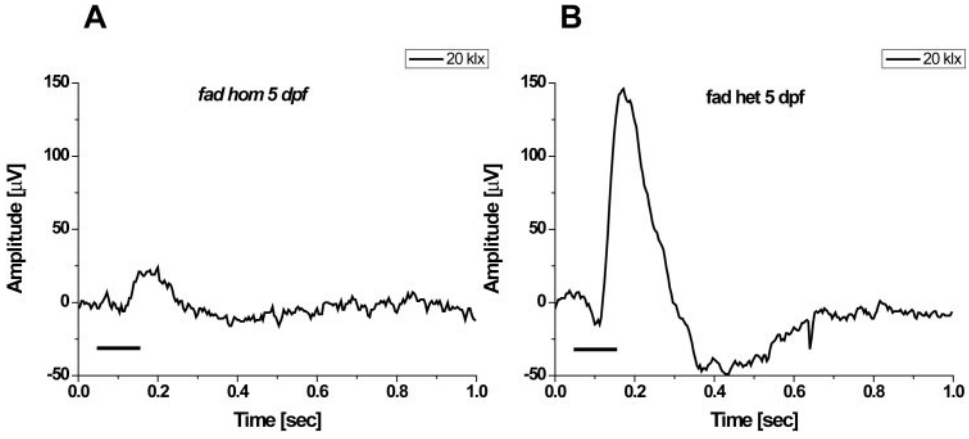

FIGURE 3. The ERG b-wave was reduced in the *fad* mutant. Representative averaged traces of ERG records from *fad* (**A**) and siblings (**B**) under the dark-adapted state. The b-wave amplitude was reduced, and light stimulus intensity in *fad* mutants increased. The *fad* mutants resulted in a significant reduction in the b-wave (univariate ANOVA [UNIANOVA]: $df = 1$; $F = 5.4$; $\alpha < 0.05$) compared with siblings over five levels of intensity (data not shown).

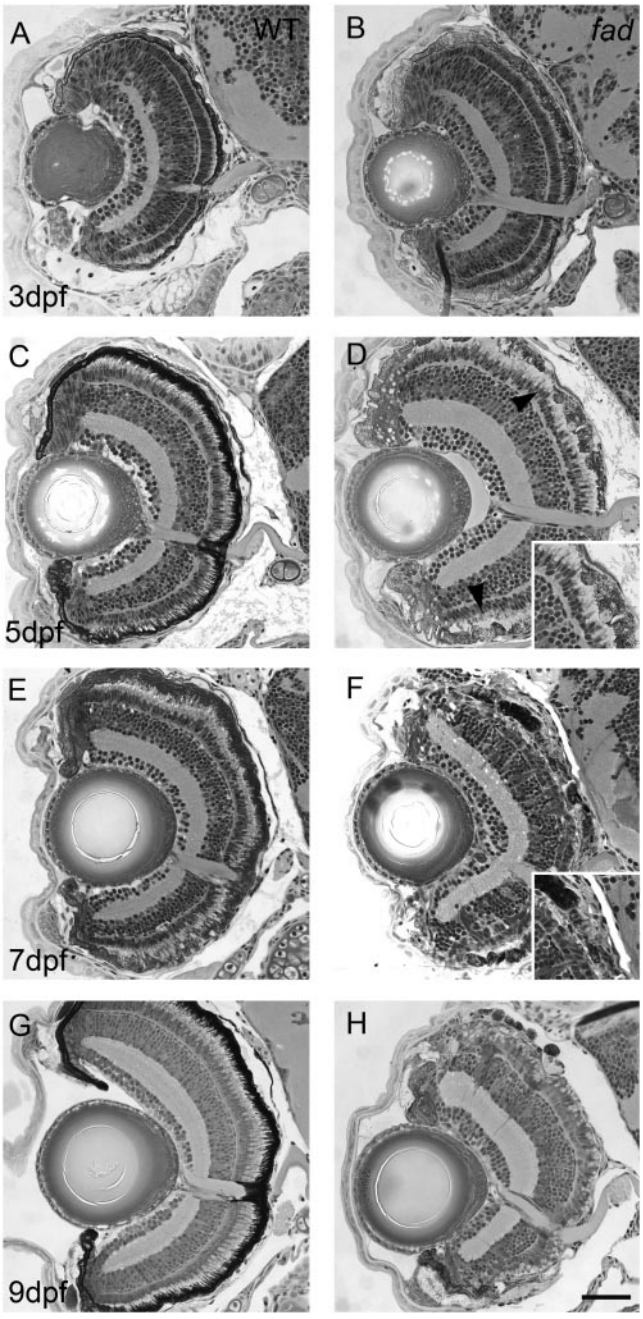

FIGURE 4. Retinal histology at different larval stages. Transverse sections through the retina in wild-type (**A**, **C**, **E**, **G**) and *fad* (**B**, **D**, **F**, **H**) larvae. At 3 dpf, wild-type (**A**) and *fad* (**B**) displayed laminated retinas, and the homozygous *fad* could not be differentiated from the heterozygous sibling. At 5 dpf, the retina of the wild-type was densely pigmented, and the PRC outer segments were clearly visible (**C**). In *fad* retinas, the RPE appeared hypopigmented (**D**, *inset*), and the PRC outer segments were shorter (*arrowheads* in **D**). At 7 dpf (**F**), the RPE was progressively more affected. In contrast to wild-type cells, RPE cells appeared to be hypopigmented, and PRC outer segments were severely shortened or absent (**F**, *inset*). At 9 dpf, the wild-type RPE had marked pigmentation, and the photoreceptor outer segments were strongly elongated (**G**), whereas mutant RPE cells lost their pigmentation and only few pigmented cells were detectable at the periphery. Additionally, outer segments were absent or barely visible (**H**). Scale bar: 50 μm.

To test whether cell death levels were elevated, we used the in situ TUNEL method for DNA fragmentation as an assay for apoptosis.[29] Consistent with previously published results, we observed few apoptotic cells in the wild-type retina[30] (Fig. 6). In the mutant retina, more apoptotic cells were observed in the outer nuclear layer at 5 dpf (Fig. 6B). The increase of apoptotic cells in the outer retina was highly significant at 6 dpf (homozygous *fad* larvae: 5.5 ± 4.6; wild-type: 0.45 ± 0.47; $P < 0.0001$; $n = 10$; Fig. 6D). No significant increase was observed in the inner retina. At earlier stages, the amount of apoptotic cells in the *fad* mutant was not significantly different from that of the wild-type retina. At later developmental stages (between 7 and 9 dpf), few cells died through an apoptotic cell death

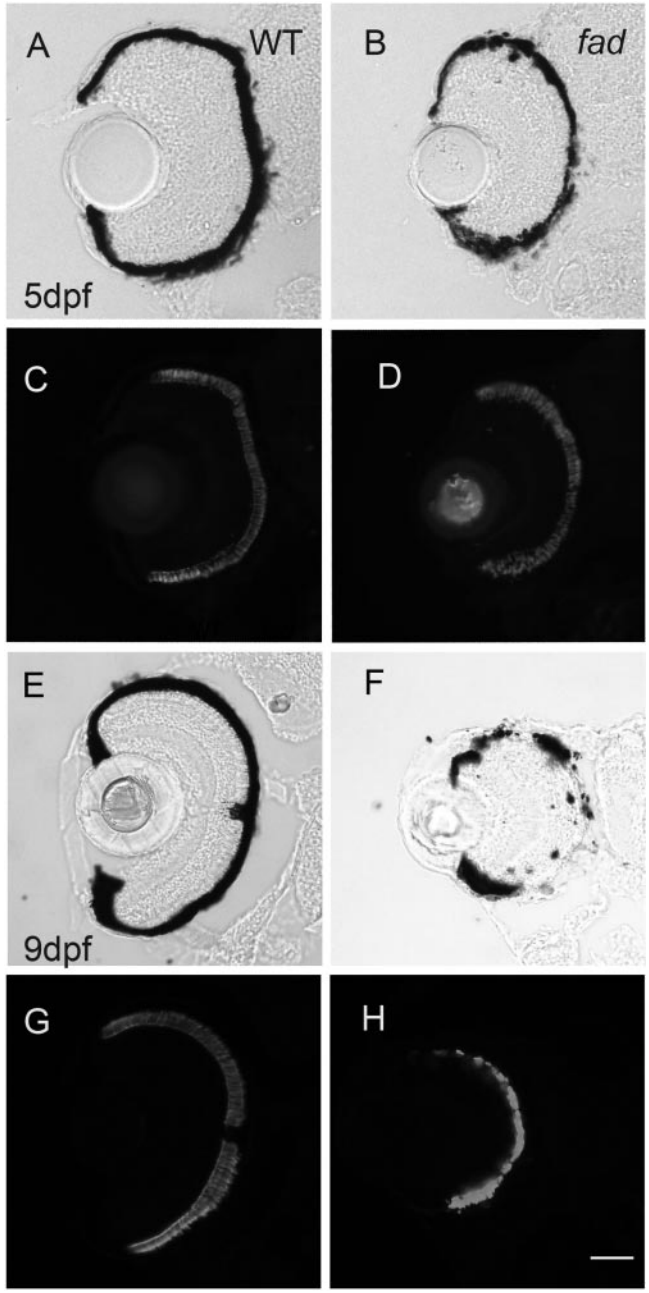

FIGURE 5. Double-cone–specific labeling of wild-type and *fad* retinas at 5 and 9 dpf. Transverse sectioning through the retinas of wild-type and *fad*. Bright-field images of the wild-type retina at 5 dpf (**A**) and at 9 dpf (**E**). *fad* mutant at 5 dpf (**B**) 9 dpf (**F**). Wild-type (**C**, **G**) and *fad* (**D**, **H**) mutant retinas stained with zpr1 antibody at 5 dpf and 9 dpf, respectively. In the *fad* mutant photoreceptor, immunoreactivity is at 5 dpf (**D**) and is present but progressively decreased at 9 dpf (**H**). Scale bar: 50 μm.

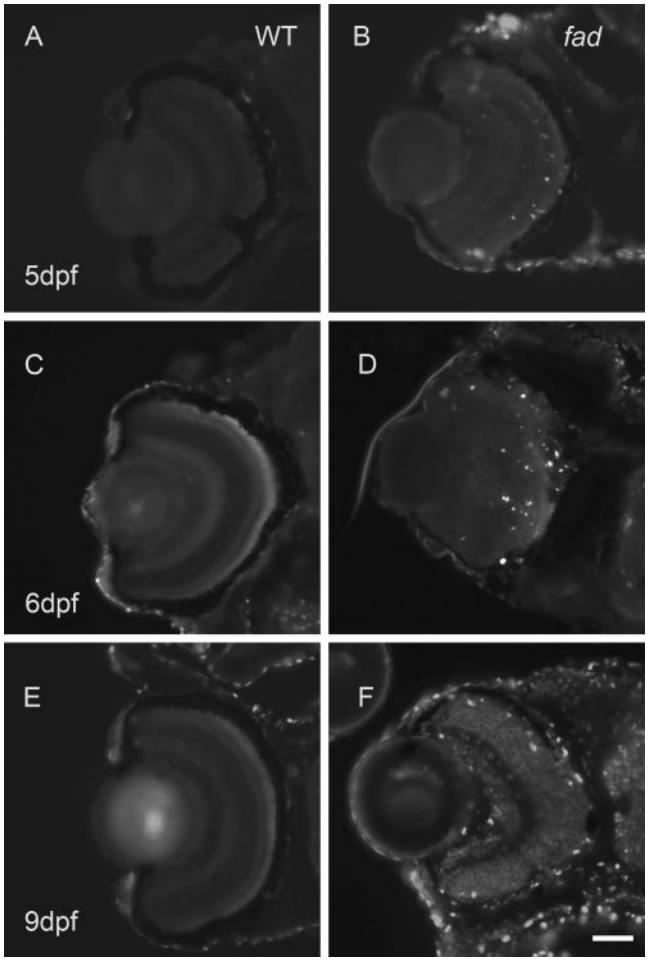

FIGURE 6. TUNEL labeling of apoptotic cells in the transverse section of wild-type (WT; **A**, **C**, **E**) and *fad* (**B**, **D**, **F**) retinas. At 6 dpf, a dramatic increase in apoptotic cells in the outer retina of the mutant retina became apparent (**D**). At later stages, fewer cells died because few cells in the outer retina remained. Scale bar: 50 μm.

pathway because few cells were left in the outer nuclear layer. In the *fad* mutant, apoptotic cell death was mainly concentrated in the outer retinal layer.

Ultrastructural Analysis of the *fad* Retina

Histologic analysis revealed defects in the RPE and the outer segments of PRCs. To examine ultrastructure defects of RPE and PRC outer segments, we performed thin-section transmission electron microscopy (TEM) at different developmental stages between 3 and 9 dpf. At 3 dpf, melanosomes exhibited normal morphology and were round, and the retina of *fad* mutant could not be differentiated from that of its wild-type sibling (Fig. 7A, 7B). The RPE of 5-day-old *fad* mutant larva contained fewer and smaller melanosomes (Fig. 7D).

The characteristic microvilli of RPE cells that interdigitate with the outer segments of the photoreceptors are rarely detected in 5 dpf and older *fad* larvae (Fig 7C, arrow). Because these microvilli are instrumental for the function, maintenance, and structural stabilization of rod and cone outer segments of PRCs,[17] their absence suggested a ready explanation for the misaligned and shorter PRC outer segments at older larval stages. Starting at 5 dpf, PRC outer segments became shorter and were partially misaligned (Fig. 7D). At 7 dpf, PRC outer segments were no longer aligned and were reduced or absent, whereas the inner segments appeared to be unaffected (Fig. 7F). Cells of the inner retina also appeared to be unaffected. Nevertheless, we clearly observed black pigment in RPE and skin melanophores, suggesting that *fad* does not affect melanin synthesis but, rather, its deposition.

The phagocytic activity of the RPE was unaffected; we frequently found vesicles with enclosed PRC outer segment

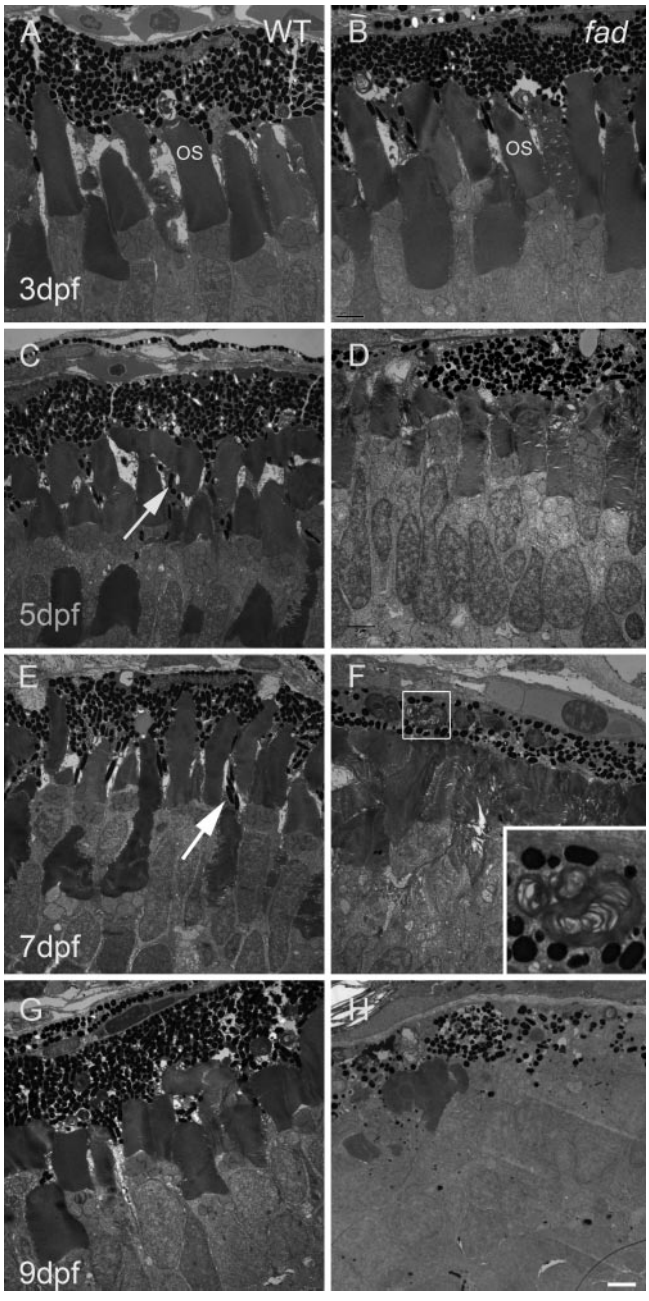

FIGURE 7. Electron micrographs of transverse sections of wild-type (WT) and *fad* outer retina. Sections were taken from (**A**, **B**) 3 dpf, (**C**, **D**) 5 dpf, (**E**, **F**) 7 dpf, and (**G**, **H**) 9 dpf. At 3 dpf, the retina of *fad* (**B**) could not be differentiated from that of heterozygous siblings (**A**). At 5 dpf, the outer segments of photoreceptors were shorter and partially misaligned in the mutant (**D**). Phagocytosis of the shed disks seemed not to be compromised (**F**, *inset*). Microvilli that stabilize the outer segments of the wild-type (**E**, *arrow*) are rarely found in the *fad* mutants (**F**). Two days later, at 9 dpf, the RPE disintegrated and the photoreceptor outer segments were strongly reduced or absent (**H**). OS, outer segments of PRCs. Scale bar: 2 μm.

TABLE 1. Comparison of Human and Zebrafish *Hps* Orthologous Genes

Gene	Zebrafish Chromosome	Closest Marker on the Zebrafish Chromosome (distance)	Human Chromosome
Hps1	2	zc115o21.za (28 cR)	10q23.1
Hps2	10	fj48d04.x1 (8 cR)	5q14.1
Hps3	22	z9817 (4 cR)	3q24
Hps4	8	fc47b02 (3 cR)	22q11.2-q12.2
Hps5	25	zc87l10.za (10 cR)	11p15-p13
Hps6	21	fk36h07 preliminary data taken from ensemble zebrafish database	10q24.32
Hps7	13	fi20h05.x1 (4 cR)	6p22.3

fragments in the RPE (Fig. 7F, inset). The defect in the outer retina was progressive. By 9 dpf, few PRC outer segments were left, and the RPE disintegrated.

Prolongation of Blood Vessel Occlusion

Because HPS was associated with defects in platelet function, we measured TTO of the dorsal aorta in *fad* mutant larvae after laser injury as a measure of platelet defect because thrombocytes are equivalents of mammalian platelets, and their intact function is essential for complete arterial occlusion in a predetermined amount of time. During laser-induced injury, thrombocytes become activated and adhere to the subendothelial surface. Subsequently, other thrombocytes aggregate at the injured site, culminating in vascular occlusion.[40] Any defect in thrombocyte function would lead to reduced thrombocyte aggregation; thus, vessel occlusion takes longer. Therefore, prolongation of TTO is an indication of thrombocyte function. To assess whether the *fad* mutants have HPS-like characteristics with respect to platelet defects, we selected 24 larvae from each of two batches and subjected them to laser injury and measured TTO and compared that time with TTO from controls. The average TTO from the control larvae was 41 seconds and that from *fad* mutants was 53 seconds ($n = 24$). This was considered to indicate a mild defect because we arbitrarily classified longer than 1 minute as indicating a severe defect.

Candidate Gene Linkage Analysis

In a first step to elucidate the molecular nature of the *fad* mutant, we mapped the locus onto the zebrafish genome by SSLP mapping.[32] Analysis of 800 meioses resulted in a map position linkage group 2 that was 1.4 cM from SSLP marker z10050.

Because the phenotype of *fad* has all the characteristics of HPS, we used the human and mouse sequences to identify zebrafish orthologs. We could identify zebrafish orthologs of all seven HPS genes in zebrafish by alignment to EST databases or to the zebrafish genomic sequence. Primers against the genomic sequence of these genes were designed, and amplicons were mapped on the Goodfellow T51 RH panel.[34] None of these ortholog genes mapped to the same chromosome as the *fad* mutation (Table 1). Therefore, we concluded that *fad* was likely caused by a mutation in a novel HPS gene, presumably involved in vesicle biogenesis or trafficking.

DISCUSSION

In this study we characterized visual defects in the hypopigmented zebrafish mutant (*fade out*). The recessive mutant was initially isolated because of its lighter body pigmentation, which also affected the RPE.[22] Additional defects in visual performance have been uncovered by a behavioral screen based on assaying the optokinetic nystagmus and the optomotor response, two innate, visually mediated behaviors.[24]

Here we describe morphologic defects in melanin-containing melanosomes of the RPE. Ultrastructural analysis revealed RPE cells that were hypopigmented as a result of a progressive decrease in melanosome size and number. The presence of melanin argues for a defect in intraorganelle melanin organization rather than melanin synthesis. RPE cells also develop tiny or small microvilli.

Histologic analysis indicated dramatic morphologic changes of the abutting PRCs, manifested by shorter and misaligned outer segments, ultimately leading to apoptotic cell death with a peak at 6 dpf. PRCs and RPE cells interact in multiple ways,[20] and several studies have shown that this interaction is crucially involved in the maintenance of photoreceptors.[16] Hence, we deem it likely that the primary defect in the *fad* visual system lies in the RPE, secondarily affecting photoreceptor morphology and survival. However, not all RPE function is abolished because we found evidence for intact phagocytosis of photoreceptor outer segments by the RPE. We recently identified the gene defect causing a similar retinal defect in the *fading vision* mutant. In this mutant, the causative *silver a* gene is exclusively expressed in RPE cells, consistent with the possibility that an RPE-specific gene defect can cause the observed deficits in the PRC layer.[18] However, we cannot exclude the possibility that the *fad* gene product is needed in RPE and photoreceptors.

The observed morphologic changes in the outer retina led to a progressive loss of vision, evidenced by diminished or absent ERG response and reduced optokinetic responses.

Apart from defects in melanogenic cells, we also found a significant prolonged bleeding time by an assay for TTO.[40] This triad of phenotypes is characteristic of HPS in humans[1–3]; defects in seven genes can cause it. These genes are thought to function in intracellular biogenesis and trafficking of late LROs. These organelles encompass melanosomes and platelet-dense granules. In humans, most of the HPS genes are members of three protein complexes, termed biogenesis of lysosome-related organelles complexes (BLOCs). BLOC-1 contains *Hps*7,[31]

BLOC-2 contains the protein products of *Hps3*, *Hps5*, and *Hps6*,[41–43] and BLOC-3 contains the proteins encoded by the *Hps1* and *Hps4* genes.[44–46] The remaining *Hps2* gene product encodes for the β_3A subunit gene (*ADTB3A*) of the AP-3 adaptor complex, involved in intracellular vesicle docking.[47,48]

These data readily suggest a cellular mechanism for the phenotype in *fad* mutant embryos and candidate genes. We therefore cloned the zebrafish ortholog of the human HPS genes and compared their genomic localization with the *fad* locus. For all human genes, we found one ortholog in the zebrafish that could be unequivocally mapped on the genome. Given that we found only one orthologous zebrafish HPS gene for each human gene, it is likely that duplicated paralogues created by the genome duplication in the lineage divergence of ray- and lobe-finned fish[49,50] have been subsequently purged from the genome.

We found no cosegregation between the *fad* locus and the seven HPS genes; therefore, we propose that *fad* encodes a novel HPS-like gene, likely involved in biogenesis or trafficking of LROs. This somewhat mirrors the situation in the mouse, in which 14 loci have been associated with HPS but only 7 have been associated with a human disease.[21] Our preliminary data have found no cosegregation of *fad* with any of the additional mouse HPS loci (data not shown). It is unclear why humans seem to have fewer HPS-causing genes than mouse and, presumably, zebrafish. It could well be that mutations in these genes are incompatible with human fetal development and are absent in the patient population. Alternatively, future genetic screening of patient populations might reveal additional, rarer human HPS genes.

Our data provide strong evidence for involvement of the *fad* gene product in late LRO function. Disruption of this process leads to cellular changes in RPE cells, such as the absence of microvilli, which in turn negatively affect PRC morphology and function. However, we have little understanding of how a defect in LRO function leads to such dramatic cellular changes. Perhaps even more surprising is the case of the *fading vision* mutant, whereby a mutation in the *silver a* gene leads to gross changes in outer retinal morphology, though the gene product may be solely involved in melanin deposition in melanosomes.[18]

In summary, we have characterized the visual defects of the *fad* zebrafish mutant and have provided evidence for the mutant as a novel animal HPS model. Our data show that the morphology of the photoreceptor is directly affected, suggesting that visual deficits in human patients might, at least in part, be caused by morphologic defects in the outer retina. To our knowledge, this is the first report of a lower vertebrate HPS model. The near future will likely see additional zebrafish mutant strains that affect LRO biogenesis, paving the way for use of the formidable genetic power of the zebrafish model to unravel the biology underlying these diseases.

Acknowledgments

The authors thank David Belet for technical assistance, Robert Geisler for allowing use of his genomic facility and for providing the Goodfellow T51 panel, and Martin Schwab and Lukas Sommer for helpful discussions and for reading the manuscript.

References

1. Hermansky F, Pudlak P. Albinism associated with hemorrhagic diathesis and unusual pigmented reticular cells in the bone marrow: report of two cases with histochemical studies. *Blood*. 1959;14:162–169.
2. Huizing M, Gahl WA. Disorders of vesicles of lysosomal lineage: the Hermansky-Pudlak syndromes. *Curr Mol Med*. 2002;2:451–467.
3. Huizing M, Anikster Y, Gahl WA. Hermansky-Pudlak syndrome and related disorders of organelle formation. *Traffic*. 2000;1:823–835.
4. Iwata F, Reed GF, Caruso RC, Kuehl EM, Gahl WA, Kaiser-Kupfer MI. Correlation of visual acuity and ocular pigmentation with the 16-bp duplication in the HPS-1 gene of Hermansky-Pudlak syndrome, a form of albinism. *Ophthalmology*. 2000;107:783–789.
5. Simon JW, Adams RJ, Calhoun JH, Shapiro SS, Ingerman CM. Ophthalmic manifestations of the Hermansky-Pudlak syndrome (oculocutaneous albinism and hemorrhagic diathesis). *Am J Ophthalmol*. 1982;93:71–77.
6. Summers CG, Knobloch WH, Witkop CJ Jr, King RA. Hermansky-Pudlak syndrome: ophthalmic findings. *Ophthalmology*. 1988;95:545–554.
7. Gahl WA, Brantly M, Kaiser-Kupfer MI, et al. Genetic defects and clinical characteristics of patients with a form of oculocutaneous albinism (Hermansky-Pudlak syndrome). *N Engl J Med*. 1998;338:1258–1264.
8. Witkop CJ, Krumwiede M, Sedano H, White JG. Reliability of absent platelet dense bodies as a diagnostic criterion for Hermansky-Pudlak syndrome. *Am J Hematol*. 1987;26:305–311.
9. Di Pietro SM, Dell'Angelica EC. The cell biology of Hermansky-Pudlak syndrome: recent advances. *Traffic*. 2005;6:525–533.
10. Huizing M, Boissy RE, Gahl WA. Hermansky-Pudlak syndrome: vesicle formation from yeast to man. *Pigment Cell Res*. 2002;15:405–419.
11. Shotelersuk V, Hazelwood S, Larson D, et al. Three new mutations in a gene causing Hermansky-Pudlak syndrome: clinical correlations. *Mol Genet Metab*. 1998;64:99–107.
12. Dell'Angelica EC, Mullins C, Caplan S, Bonifacino JS. Lysosome-related organelles. *FASEB J*. 2000;14:1265–1278.
13. Israels SJ, McNicol A, Robertson C, Gerrard JM. Platelet storage pool deficiency: diagnosis in patients with prolonged bleeding times and normal platelet aggregation. *Br J Haematol*. 1990;75:118–121.
14. White JG. The dense bodies of human platelets: inherent electron opacity of the serotonin storage particles. *Blood*. 1969;33:598–606.
15. McNicol A, Israels SJ. Platelet dense granules: structure, function and implications for hemostasis. *Thromb Res*. 1999;95:1–18.
16. Strauss O. The retinal pigment epithelium in visual function. *Physiol Rev*. 2005;85:845–881.
17. Marmorstein AD, Finnemann SC, Bonilha VL, Rodriguez-Boulan E. Morphogenesis of the retinal pigment epithelium: toward understanding retinal degenerative diseases. *Ann NY Acad Sci*. 1998;857:1–12.
18. Schonthaler HB, Lampert JM, von Lintig J, Schwarz H, Geisler R, Neuhauss SC. A mutation in the silver gene leads to defects in melanosome biogenesis and alterations in the visual system in the zebrafish mutant fading vision. *Dev Biol*. 2005;284:421–436.
19. Bok D. Retinal photoreceptor-pigment epithelium interactions: Friedenwald lecture. *Invest Ophthalmol Vis Sci*. 1985;26:1659–1694.
20. Bok D. The retinal pigment epithelium: a versatile partner in vision. *J Cell Sci Suppl*. 1993;17:189–195.
21. Li W, Rusiniak ME, Chintala S, Gautam R, Novak EK, Swank RT. Murine Hermansky-Pudlak syndrome genes: regulators of lysosome-related organelles. *Bioessays*. 2004;26:616–628.
22. Kelsh RN, Brand M, Jiang YJ, et al. Zebrafish pigmentation mutations and the processes of neural crest development. *Development*. 1996;123:369–389.
23. Haffter P, Nusslein-Volhard C. Large scale genetics in a small vertebrate, the zebrafish. *Int J Dev Biol*. 1996;40:221–227.
24. Neuhauss SC, Biehlmaier O, Seeliger MW, et al. Genetic disorders of vision revealed by a behavioral screen of 400 essential loci in zebrafish. *J Neurosci*. 1999;19:8603–8615.
25. Brand MG, Nüsslein-Volhard CH. Keeping and raising zebrafish. In: Nusslein-Volhard CH, Dahm R, eds. *Zebrafish, Practical Approach Series*. Oxford, UK: Oxford University Press; 2002:7–37.
26. Kimmel CB, Ballard WW, Kimmel SR, Ullmann B, Schilling TF. Stages of embryonic development of the zebrafish. *Dev Dyn*. 1995;203:253–310.

27. Rinner O, Rick JM, Neuhauss SC. Contrast sensitivity, spatial and temporal tuning of the larval zebrafish optokinetic response. *Invest Ophthalmol Vis Sci*. 2005;46:137–142.
28. Makhankov YV, Rinner O, Neuhauss SC. An inexpensive device for non-invasive electroretinography in small aquatic vertebrates. *J Neurosci Methods*. 2004;135:205–210.
29. Gavrieli Y, Sherman Y, Ben-Sasson SA. Identification of programed cell death in situ via specific labeling of nuclear DNA fragmentation. *J Cell Biol*. 1992;119:493–501.
30. Biehlmaier O, Neuhauss SC, Kohler K. Onset and time course of apoptosis in the developing zebrafish retina. *Cell Tissue Res*. 2001; 306:199–207.
31. Li W, Zhang Q, Oiso N, et al. Hermansky-Pudlak syndrome type 7 (HPS-7) results from mutant dysbindin, a member of the biogenesis of lysosome-related organelles complex 1 (BLOC-1). *Nat Genet*. 2003;35:84–89.
32. Geisler R. Mapping and cloning. In: Nusslein-Volhard C, Dahm R, eds. *Zebrafish, Practical Approach Series*. Oxford, UK: Oxford University Press; 2002:175–212.
33. Altschul SF, Madden TL, Schaffer AA, et al. Gapped BLAST and PSI-BLAST: a new generation of protein database search programs. *Nucleic Acids Res*. 1997;25:3389–3402.
34. Geisler R, Rauch GJ, Baier H, et al. A radiation hybrid map of the zebrafish genome. *Nat Genet*. 1999;23:86–89.
35. Easter SS Jr, Nicola GN. The development of vision in the zebrafish (*Danio rerio*). *Dev Biol*. 1996;180:646–663.
36. Branchek T. The development of photoreceptors in the zebrafish, *Brachydanio rerio*, II: function. *J Comp Neurol*. 1984;224:116–122.
37. Schmitt EA, Dowling JE. Early retinal development in the zebrafish, *Danio rerio*: light and electron microscopic analyses. *J Comp Neurol*. 1999;404:515–536.
38. Larison KD, Bremiller R. Early onset of phenotype and cell patterning in the embryonic zebrafish retina. *Development*. 1990; 109:567–576.
39. Peterson RE, Fadool JM, McClintock J, Linser PJ. Müller cell differentiation in the zebrafish neural retina: evidence of distinct early and late stages in cell maturation. *J Comp Neurol*. 2001;429:530–540.
40. Gregory M, Hanumanthaiah R, Jagadeeswaran P. Genetic analysis of hemostasis and thrombosis using vascular occlusion. *Blood Cells Mol Dis*. 2002;29:286–295.
41. Di Pietro SM, Falcon-Perez JM, Dell'Angelica EC. Characterization of BLOC-2, a complex containing the Hermansky-Pudlak syndrome proteins HPS3, HPS5 and HPS6. *Traffic*. 2004;5:276–283.
42. Gautam R, Chintala S, Li W, et al. The Hermansky-Pudlak syndrome 3 (cocoa) protein is a component of the biogenesis of lysosome-related organelles complex-2 (BLOC-2). *J Biol Chem*. 2004;279: 12,935–942.
43. Zhang Q, Zhao B, Li W, et al. Ru2 and Ru encode mouse orthologs of the genes mutated in human Hermansky-Pudlak syndrome types 5 and 6. *Nat Genet*. 2003;33:145–153.
44. Chiang PW, Oiso N, Gautam R, Suzuki T, Swank RT, Spritz RA. The Hermansky-Pudlak syndrome 1 (HPS1) and HPS4 proteins are components of two complexes, BLOC-3 and BLOC-4, involved in the biogenesis of lysosome-related organelles. *J Biol Chem*. 2003;278: 20,332–337.
45. Martina JA, Moriyama K, Bonifacino JS. BLOC-3, a protein complex containing the Hermansky-Pudlak syndrome gene products HPS1 and HPS4. *J Biol Chem*. 2003;278:29,376–384.
46. Nazarian R, Falcon-Perez JM, Dell'Angelica EC. Biogenesis of lysosome-related organelles complex 3 (BLOC-3): a complex containing the Hermansky-Pudlak syndrome (HPS) proteins HPS1 and HPS4. *Proc Natl Acad Sci USA*. 2003;100:8770–8775.
47. Dell'Angelica EC, Shotelersuk V, Aguilar RC, Gahl WA, Bonifacino JS. Altered trafficking of lysosomal proteins in Hermansky-Pudlak syndrome due to mutations in the beta 3A subunit of the AP-3 adaptor. *Mol Cell*. 1999;3:11–21.
48. Feng L, Seymour AB, Jiang S, et al. The beta3A subunit gene (Ap3b1) of the AP-3 adaptor complex is altered in the mouse hypopigmentation mutant pearl, a model for Hermansky-Pudlak syndrome and night blindness. *Hum Mol Genet*. 1999;8:323–330.
49. Gates MA, Kim L, Egan ES, et al. A genetic linkage map for zebrafish: comparative analysis and localization of genes and expressed sequences. *Genome Res*. 1999;9:334–347.
50. Postlethwait JH, Woods IG, Ngo-Hazelett P, et al. Zebrafish comparative genomics and the origins of vertebrate chromosomes. *Genome Res*. 2000;10:1890–1902.